ISSN (Print) 1226-5268 ISSNS (Online) 2287-7169
The Journal of Engineering Geology, Vol.24, No.3, September, 2014, pp. 323-332
http://dx.doi.org/10.9720/kseg.2014.3.323

3D Finite Element Analysis of Fault Displacements in the Nobi Fault Zone, Japan

Young-Mook Choi[1], Woo-Seok Kim[1], Chul-Goo Lee[1], Chang-Yong Kim[2], and Yong-Seok Seo[1,*]

[1]Department of Earth and Environmental Sciences, Chungbuk National University
[2]Geotechnical Engineering and Tunnelling Research Division,
Korea Institute of Construction Technology (KICT)

Received 4 August 2014; received in revised form 25 August 2014; accepted 28 August 2014

The Nobi fault zone, which generated the 1891 Nobi Earthquake (M8.0), includes five or six faults distributed in and around Gifu and Aichi prefectures, Japan. Because large cities are located near the fault zone (e.g., Gifu and Nagoya), and because the zone will likely be reactivated in the future, relatively thorough surveys have been conducted on the 1891 Nobi earthquake event, examining the fault geometry, house collapse rate, and the magnitude and distribution of earthquake intensity and fault displacement. In this study, we calculated the earthquake slip along faults in the Nobi fault zone by applying a 3D numerical analysis. The analysis shows that a zone with slip displacements of up to 100 mm included all areas with house collapse rates of 100%. In addition, the maximum vertical displacement was approximately ± 1700 mm, which is in agreement with the ± 1400 mm or greater vertical displacements obtained in previous studies. The analysis yielded a fault zone with slip displacements of > 30 mm that is coincident with areas in which house collapse rates were 60% of more. The analysis shows that the regional slip sense was coincident with areas of uplift and subsidence caused by the Nobi earthquake.

Key words : 1891 Nobi earthquake, seismic fault, house collapse rate, surface displacement, 3D numerical analysis

Introduction

Unlike the regions of Japan and China, which include plate boundaries, the Korean Peninsula, which is located within the Eurasia plate, is an area of small- to medium-sized earthquakes exhibiting relatively large recurrence intervals. However, Quaternary faults have recently been identified in the southeastern part of the Korean Peninsula, and studies are currently under way to estimate their rupture lengths, as well as the magnitudes of associated paleoearthquake events based on displacements measured in the field (Kim and Jin, 2006, 2007). The evaluation of the maximum magnitudes of paleoearthquakes based on paleoseismological data will provide a basis for predicting the magnitudes of possible future earthquakes (Kyung, 2010). At the same time, studies are being conducted to appraise the magnitudes of past and future earthquakes by means of probabilistic methods (Chang and Park, 2010; Yeon et al., 2010). Such methods can overcome some of the limitations of field-based studies, which derive earthquake magnitude data by deterministic methods, and which are hence subject to variations and uncertainties related to field-based measurements of fault parameters. Most analyses of displacement, strain rate, stress, and other parameters caused by faulting rely on numerical analysis methods based on the Coulomb program (Lin and Stein,

*Corresponding author: ysseo@cbu.ac.kr

2004; Toda et al., 2005) developed by the United States Geological Society (USGS). Ko et al. (2009) made it clear in their study entitled "Odaesan Earthquake and Its Aftershock Distribution" that it is possible to apply the coulomb stress model to seismic faults of medium scale located in Korea, and Han et al. (2009) have put the model to use in their modeling of the evolution of the Yangsan-Woolsan fault system. The model is advancing to the point of successful aftershock prediction, based on a knowledge of heterogeneities in materials and the mechanical properties of the fault zone (Hu et al., 2013).

While the foregoing studies have focused largely on the prediction of aftershocks, or the determination of earthquake scale, other on-gong studies seek to predict the damage to structures caused by earthquake-induced displacements. Studies on the effects of surface deformation during an earthquake and on the stability of structures include analyses of the locations of faults that could induce surface deformation, the recommended distance between nuclear power plant sites and fault zones, studies on the size of the radius of the damaged area around an earthquake epicenter (Kim et al., 2010), analyses based on 3D numerical simulations, etc. (Seo et al., 2011a, 2011b).

This study calculates earthquake-related displacement and stress based on 3D numerical analyses, and compares the results of the analyses with measurements of actual displacements and the scale of observed damage to structures. The results are evaluated in terms of their applicability to the Nobi fault zone in Japan, a source of large earthquakes that is relatively well known with regard to fault models, field data, surface displacement, and extent of earthquake-related damage.

Geology and faults

The study area, consisting of the Nobi Plain and the Nobi Fault Zone, is located in and around Gifu and Aichi prefectures, Japan. The host rocks in the area are Paleozoic limestone, chert, and sandstone, and conglomerate. Cenozoic alluvial deposits are widely distributed in the southern part of the area (Fig. 1). Topographically, the region to the north is more mountainous, while the south consists mainly of plains. In the central part of the fault zone, basaltic and pyroclastic rocks of Paleozoic–

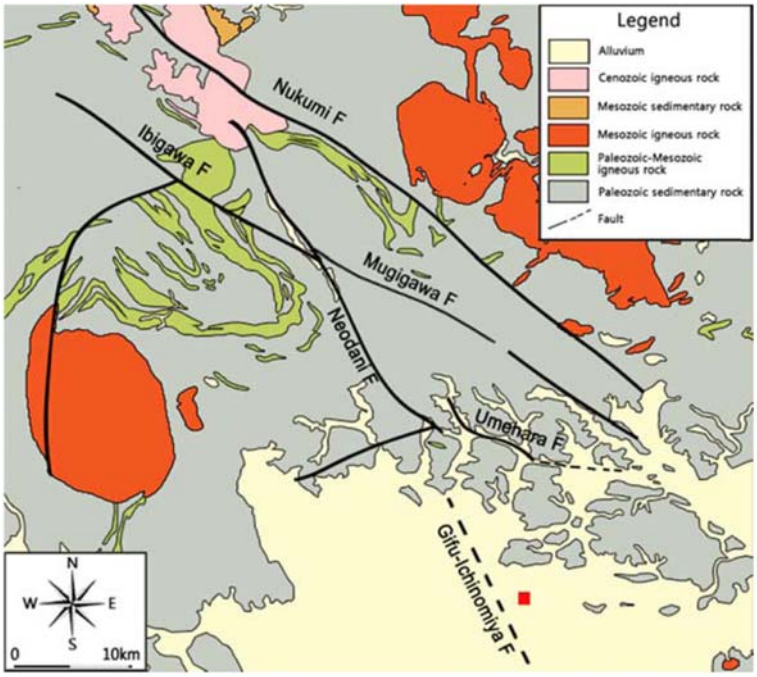

Fig. 1. Geological map of the study area (modified from Wakita et al., 1992).

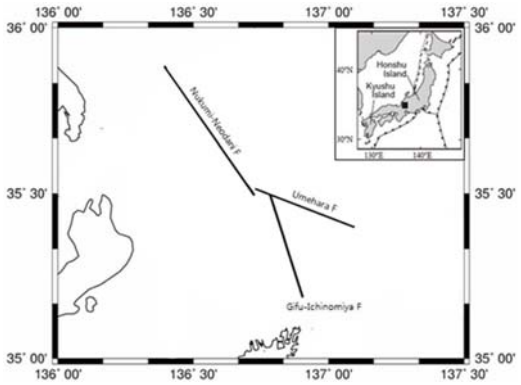

Fig. 2. Locations of fault traces associated with the 1891 Nobi earthquake (modified from Nakano et al., 2007), discussed as faults F1-F5 in the text, comprising the Nukumi-Neodani faults (faults F1-F3), the Umehara Fault (F4), and the Gifu-Ichinomiya Fault (F5).

Mesozoic age are distributed in a zonal pattern. The area outside of the fault zone comprises Mesozoic granites associated with volcanism.

Faults in the area include the Nukumi, Ibigawa, Mugigawa, Neodani, Umehara, and Gifu-Ichinomiya faults. Of these, all except the Gifu-Ichinomiya Fault belong to the Nobi fault zone (Earthquake Research Committee, 2005). The Nobi fault zone is divided generally into the Nukumi Fault (F1), the Ibigawa Fault (F2), the Mugigawa & Neodani Fault (F3), and the Umehara Fault (F4). The Gifu-Ichinomiya Fault (F5) is thought to be inactive, unrelated to recent earthquake activity (Earthquake Research Committee, 2001).

The study area was affected by the M8.0 Nobi earthquake of 28 October 1891 (Muramatsu, 1983). The Nobi earthquake is one of the largest-magnitude earthquakes known, along with the Great Hanshin earthquake in 1995 and the Fukushima earthquake in 2011, all of which occurred in Japan and were felt throughout the Japanese Islands, except in Hokaido and the southern Kyushu area (Miyakoshi et al., 2003). Nakano et al. (2007) proposed a new model of the Nobi fault zone (Fig. 2) that has a simplified fault structure compared with previous models and that describes five fault zones in the study area. In the simplified model, the strikes of faults F1-F3, F4, and F5 are N35W, N69W, and N27W, respectively. Faults F1-F4 are vertical and fault F5 dips 60° to the east. The simplified Nobi fault zone model has been used in the numerical analysis conducted in this study.

Previous studies

House collapse rate and distribution of seismic intensity

Figure 3 shows the spatial distribution of house collapse rates during the 1891 Nobi earthquake (Nakano et al., 2007) and an intensity distribution map (Earthquake Research Committee, 2001). Contour lines (Fig. 3a) show the distribution of house collapse rates (60%-100%) attributed to the earthquake. High collapse rates occur in a zone along the central part of the fault zone, in a hilly area in the north of the study area, and in the wide basin to the south, which included densely populated areas such as Gifu, Ogaki, and Ichinomiya City.

The map of intensity distribution (Fig. 3b) employs the intensity classification of the Japan Meteorological Administration (JMA) (intensity classes V-VII). The JMA intensity explanatory chart (http://www.jma.go.jp/jma/kishou/know/shindo/jma-shindo-kaisetsu.pdf) states that in intensity V Weak regions, “in wooden houses having a low seismic evaluation, tiny cracks are sometimes detected”; in intensity VI Strong regions, “large cracks are found on the wall, and buildings often tilted or fell.” A comparison of the distributions of intensity and house collapse rates shows that the intensity-V region approximately coincides with house collapse rates of 60%-80%, in an area suffering slight to medium structural damages. Regions with house collapse rates of 100% coincide with regions of intensity VI or VII. Areas of intensity VII nearly coincide with house collapse rates of 100% in the F2 fault area and in the western part of the F5 fault area.

Surface displacement

Mikumo and Ando (1976) devised a theoretical calculation of surface displacements associated with the Nobi earthquake based on actual displacement measurements. Figure 4 shows an uplift and subsidence distribution map based on the theoretical calculations. On faults F1-F4, eastern domains show subsidence while western domains show uplift. These data are based on cross sections a-b, b-

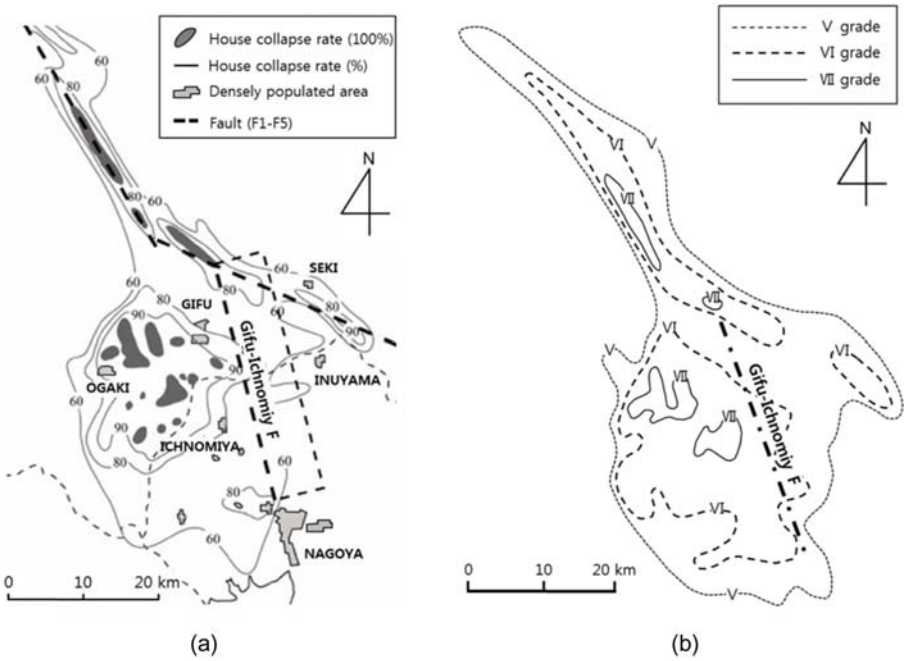

Fig. 3. (a) Distribution of house collapse rates due to the 1891 Nobi earthquake (from Nakano et al., 2007). (b) Contour map of the intensity distribution of the 1891 Nobi earthquake (modified from Earthquake Research Committee, 2001).

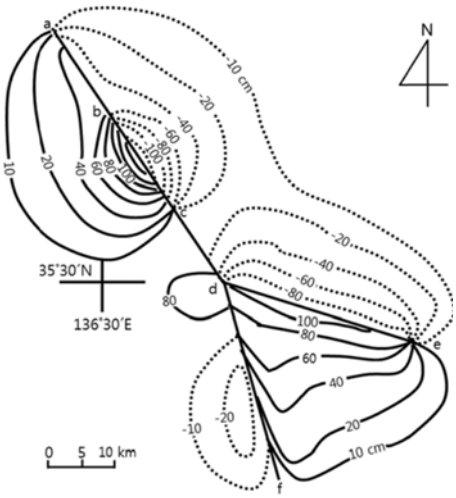

Fig. 4. Vertical displacements based on theoretical calculations and a partial survey conducted along the Nobi Fault zone. Solid and dashed contours show uplift and subsidence, respectively (modified from Mikumo and Ando, 1976). a-b: fault F1; b-c: fault F2; c-d: fault F3; d-e: fault F4; e-f fault: F5.

c, c-d, and d-e; Fig. 4). Uplift and subsidence patterns are particularly clear along fault F2. In contrast, uplift and subsidence along fault 3 are relatively minor, suggesting that as a strike-slip fault, dip-slip components are negligible.

Numerical Analysis

This study used the finite element method (FEM) to study the Nobi fault zone, based on the assumption that the fault zone can be approximated by a continuum model, and used MIDAS GTS NX, a program developed by MIDAS Information Technology Co., Ltd. MIDAS GTS NX is used worldwide for finite element analyses of 3-dimensional subsurface structures.

Analysis model

The MIDAS GTS NX can be based on a variety of material models, such as the Mohr-Coulomb, Hoek-Brown, and Drucker-Prager models. This study adopted an elasto-plasticity interpretation using a material model based on Mohr-Coulomb's failure criterion, that can be applied both on grounds and structures. The ground model applied in this study is rectangular in shape, measuring 100 km wide × 100 km long × 1.5 km deep, based on the

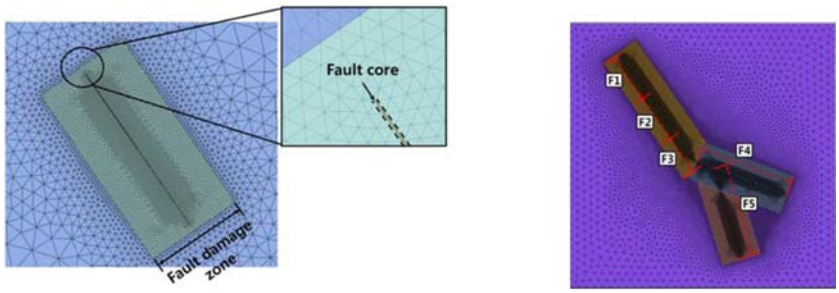

Fig. 5. A 3D finite element model (FEM) established for the numerical analysis. (a) Schematic diagram of the fault core and the damage zone, and (b) location of faults F1-F5.

Table 1. Fault parameters for each fault segment in the Nobi earthquake fault zone (from Nakano et al., 2007).

Segment	Code	Strike (°)	Dip (°)	Rake (°)	Slip (m)	Length (km)	Width (km)	Depth (km)
Nukumi	F1	145	90	45	1.4	18	15	0
Neodani (North)	F2	145	90	45	4.2	18	15	0
Neodani (South)	F3	145	90	0	7.0	16	15	0
Umehara	F4	111	90	53	1.20	35	15	0
Gifu-Ichinomiya	F5	163	60E	90	1.48	35	15	1

Table 2. Mechanical properties of bedrock, fault cores, and damage zones used in the numerical analysis.

Rock type	Elastic modulus (GPa)	Friction angle (°)	Cohesion (KPa)	Unit weight (g/cm^3)	Poisson's ratio
Host rock (Kim, 2011)	10.00	42.0	2000	2.55	0.22
Fault core (Lee, 2014)	0.12	18.0	35	1.50	0.27
Fault damage zone (Lee, 2014)	0.50	32.0	200	2.00	0.27

scale of the fault. For the fault model, the simplified F1-F5 fault model of Nakano et al. (2007) was employed (See Fig. 2); this model was derived on the basis of field data (Table 1). The fault zone can be divided into a fault core zone, a fault damage zone, and host rocks (Caine et al., 1996). The width of the fault core is shown in Fig. 5; a width of 0.02 km was applied equally to all faults, considering that preceding surveys showed that the 5 faults was 15 km wide; the real length of each fault was applied to the length of each fault, and the depth of all faults was set to 0.5 km. The damage zone was set as a rectangular area measuring 15 km wide × (length of each fault + 2 km) × 0.6 km deep, with the fault core being located in the center of the area.

Boundary conditions were established by side boundaries that bind the horizontal displacement and a lower boundary that binds vertical displacements. A self load was applied as a basic external force acting on the model as a whole. The data of Nakano et al. (2007) (Table 1) were used for the slip sense and displacement of each fault employed in the numerical analysis.

Geotechnical parameters utilized for the numerical analysis include the elastic modulus, unit weight, Poisson's ratio, friction angle, and cohesion. The analysis used geotechnical parameters for fault zones available in Korea. For parameters of host rocks used in the ground models, a median value of the geotechnical parameters was acquired through field surveys in 10 Korean sites; for the fault core and fault damage zone, geotechnical parameters were acquired through analysis of the literature (Table 2).

Results of the numerical analysis

While numerous studies have examined damage to structures caused by surface displacement as related to activities such as excavation, no risk evaluation criteria for structures are available for vertical and horizontal displacements due to faulting. Therefore, this study proposes to compare the vertical and horizontal displacements caused by earthquakes with those established as criteria for settlement of structures by building safety standards. The settlement criteria for structures vary depending on the ground mass type, and the basic form and type of the structure. The Nobi earthquake addressed in this study occurred in 1891, when most houses were presumably built with wood and clay on a simple foundation. Skempton and McDonald (1956) determined the maximum allowable settlement of a foundation as related to ground mass type, as shown in Table 3. A 32-mm settlement in the case of a sandy mass and a 45-mm settlement in the case of a clayey mass are quoted as allowable safety standards. At the same time, for a mat foundation of a cohesive soil mass, 76-127 mm is presented as an allowable value. Therefore, this study established a surface displacement of 30 mm or less as a stable domain, 30-100 mm as a damage domain, and 100 mm or more as a complete collapse domain, so as to simplify comparisons with the results of surveys for house damage.

Table 3. Limiting values for maximum settlement established for building purposes (Skempton and McDonald, 1956).

Foundation type	Settlement (mm)	
In sand	Maximum	32
In clay		45
Isolated foundations in sand	Maximum differential	51
Isolated foundations in clay		76
Raft in sand		51-76
Raft in clay		76-127

Results of the numerical analysis for surface displacements due to faulting are shown in Fig. 6; Fig. 6a shows vertical displacements on faults F1-F5. The maximum vertical displacement reached ±1700 mm in the core of fault F2; in the case of fault F3, on which the applied displacement was strike-slip only, a vertical maximum displacement of ~100 mm was calculated.

Figure 6b shows the magnitude of the vector of combined vertical and horizontal displacements on faults F1-F5. The red domain in Fig. 6b shows regions where displacements are 100 mm or greater. Progressing from fault F1 toward fault F3, the displacement domain grows wider, and displacements reach values of greater than 100 mm; also, where faults F3 and F4 overlap, the displacement domain is relatively wide. In the case of fault F5, the red domain (displacements of over 100 mm) is relatively wide. The widths of the domains (measured from the central part of the fault zone) representing up to 100-mm and 30-mm displacements are presented in Table 4. The width of the 100-mm displacement domain is least at fault F1 (~1660 m) and greatest at fault F5 (3700 m). The width of the 30-mm displacement domain, which is

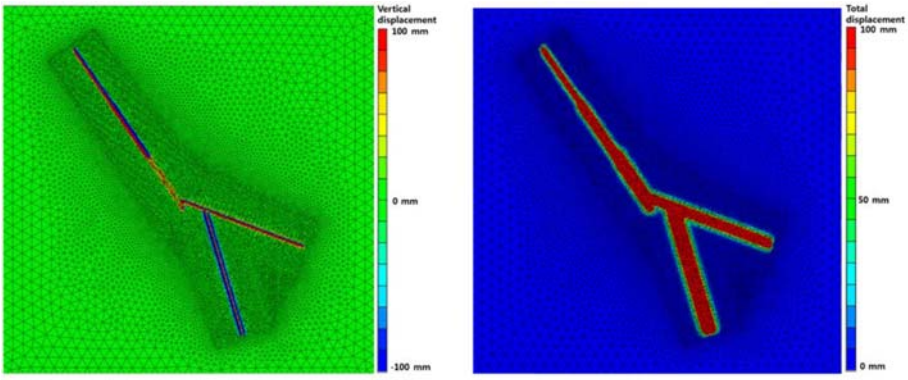

Fig. 6. Results of the numerical analysis. Distributions of (a) vertical displacement and (b) total displacement.

Table 4. Maximum width of zones with displacements of 30 and 100 mm, as calculated for each of the five faults (faults F1-F5) from the numerical analysis.

Fault	Width (m) of zone for:	
	Total displacement of up to 30 mm	Total displacement of up to 100 mm
F1	2879	1660
F2	3976	2665
F3	5046	3642
F4	4486	2669
F5	5682	3749

the house-damage criterion set earlier, is ~2800 m on fault F1 and up to 5600 m on fault F5.

Comparison of simulated and observed results

Comparison of house collapse rates

A comparison of the house collapse rates obtained by the numerical analysis and those reported by Nakano et al. (2007) shows that areas with house collapse rates of 100% are linearly distributed along the cores of faults F2-F4, and this zone of 100% collapse is wider in the southern part of the study area. Areas with house collapse rates of 100% in the domains of faults F2-F4 are located mainly in areas showing fault displacements of greater than 100 mm. In the area of fault F2, the domain with house collapse damage of over 60% has a width of ~3600 m (Fig. 7a); this is similar to the ~3976-m radius of the domain of 30-mm displacements obtained by the numerical analysis. As stated earlier, a surface settlement of 30 mm is the maximum allowable settlement of a building, which means that settlements of greater than 30 mm can cause damage to buildings. Fault displacements were not observed in the western area of fault F5 (southwestern part of Gifu), which is dotted with domains of house collapse rates of 100%, as determined by the analysis. That is, in this area, which is part of the Nobi sedimentary basin, surface soil layers are widely distributed, and analysis models are not applicable due to a lack of information on the type of underground structure.

The Nagoya area, located to the south in Fig. 7a, is a densely populated area but shows a relatively low house-collapse rate, despite being located on the extension of fault F5. This low rate can be explained by the results of the numerical analysis, which show that fault displacements are minor along the southern end of fault F5 (Fig. 7b).

Comparison of surface displacement

Figure 8 shows the theoretical magnitudes of uplift/

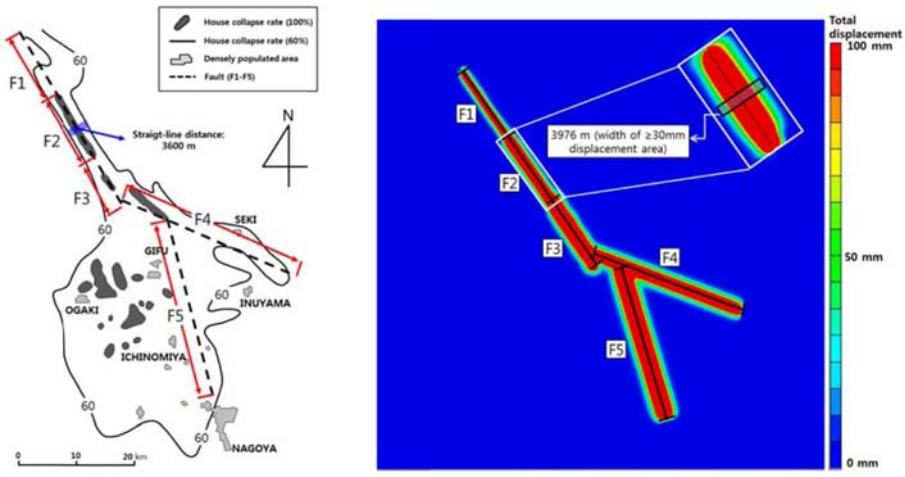

Fig. 7. Comparison of (a) house collapse rates (modified from Nakano et al., 2007) and (b) total displacements as calculated by the finite element method.

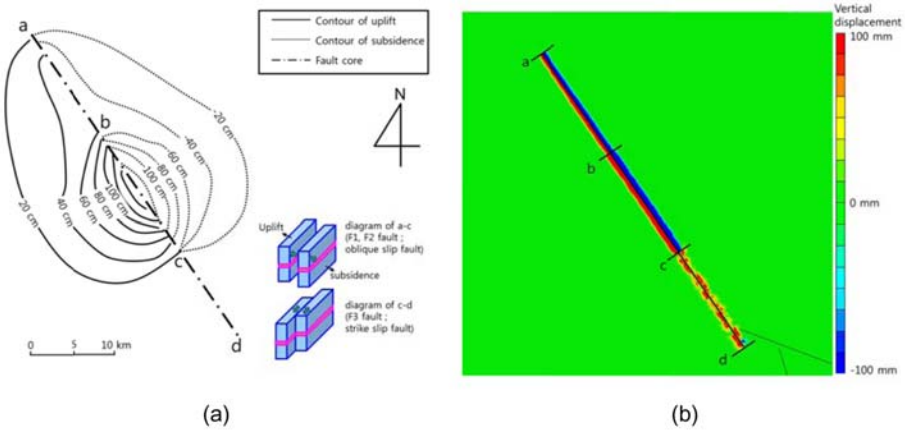

Fig. 8. Comparison of surface displacements determined by theoretical calculation (a) and those determined by the finite element method (b). a-b: fault F1; b-c: fault F2; c-d: fault F3.

subsidence (actually measured in part) determined by Mikumo and Ando (1976), and uplift/subsidence determined by the numerical analysis. The distribution and direction of uplift/subsidence determined by the two methods coincide along faults F1-F3. On faults F1 and F2, the numerical analysis shows a region of vertical displacement in the western and eastern domains centering on the fault core. Moreover, Fig. 8a shows that the regions of peak uplift and subsidence are in the core of fault F2, which is similar to the region of maximum displacement as determined by the numerical analysis.

In the case of fault F3, which is a strike-slip fault with nearly no dip-slip component, only horizontal displacements were measured, and no displacements were determined by the theoretical calculations (Mikumo and Ando, 1976). In the numerical analysis, displacements of up to ~100 mm were calculated, apparently because stresses occurring between faults F2 and F4 affected the displacement values.

Conclusions

This study examined the characteristics and distribution of fault displacement, focusing on the Nobi fault zone, by applying a numerical analysis model incorporating fault data acquired in preceding studies. According to the numerical analysis, the zone of fault displacement greater than 100 mm includes all areas showing total collapse of houses in the 1891 Nobi earthquake (i.e., a collapse rate of 100%). The numerical analysis yielded a maximum vertical displacement on fault F2 of ±1700 mm, while results of a theoretical formula that reflect actual measurement values indicate displacements of greater than 1400 mm; therefore, the results of the two approaches are relatively similar. The width of the zone of house collapse rates greater than 60% reached about 3600 m from the core of the fault, a value similar to the zone of displacements greater than 30 mm, and a region in which houses can be damaged, according to building standards. The distribution and direction of uplift/subsidence reported in preceding studies and the direction and amount of vertical displacement as determined by the numerical analysis also agree with one another. However, in domains where ground information is unavailable, such as in the Nobi Plain area, the results of the preceding studies and those of the numerical analysis are not in satisfactorily agreement.

Few studies have examined the effects of displacement caused by faulting on the ground or underground structure, the reason being that it is difficult to precisely characterize structural geologic information needed for a stability analysis, such as ground mass characteristics, the geometry of faults, displacement domains, asperities on fault planes, and stress orientations in fault zones. In the numerical model used in this study, properties of rock masses were applied in a simplified manner, disregarding alluvial

deposits, weathering zones, and so forth. However, in cases where the foregoing information has been available in the field or in the lab, recent advances in numerical analysis techniques mean that the numerical realizations have made substantial progress in the realm of displacement analysis.

Acknowledgment

This research was supported by a grant (13SCIPC 069074-01) from the Ministry of Land, Infrastructure and Transport of Korean government.

References

Caine, J. S., Evans, J. P., and Forster, C. B., 1996, Fault zone architecture and permeability structure, Geology, 24, 1025-1028.

Chang, C. J. and Park, D. H., 2010, Estimation of probabilistic paleomagnitude from the fault sources, Proceedings of KSEG Conference 2010, 261-265 (in Korean).

Earthquake Research Committee, 2001, Report on assessment of the gifu-ichinomiya fault zone, Headquarters for Earthquake Research Promotion, 12p (in Japanese).

Earthquake Research Committee, 2005, Report on assessment of the nobi fault zone, Headquarters for Earthquake Research Promotion, 49p (in Japanese).

Han, S. R., Park, J. Y., and Kim, Y. S., 2009, Evolution modeling of the Yangsan-Ulsan fault system with stress changes, Journal of the Geological Society of Korea, 45(4), 361-377 (in Korean with English abstract).

Hu, C., Cai, Y., Liu, M., and Wang, Z., 2013, Aftershocks due to property variations in the fault zone: A mechanical model, Tectonophysics, 588, 179-188.

Japan Meteorological Association, JMA intensity scale related commentary, http://www.jma.go.jp/jma/kishou/know/shindo/jma-shindo-kaisetsu.pdf (in Japanese).

Kim, H. G, 2011, 3D numerical analysis on the prediction of pre-displacement and total displacement influenced by the monitoring time of tunnel crown settlement, MSc Thesis, Chungbuk National University, 23-31 (in Korean with English abstract).

Kim, Y. S., Choi, J. H., Jin, K. M., and Shim, T. M., 2010, Importance of surface deformation and respect distance in nuclear facility sites, Proceedings of KSEG conference 2010, 47-51 (in Korean).

Kim, Y. S. and Jin, K. M., 2006, Estimated earthquake magnitude from the Yugye Fault displacement on a trench section in Pohang, Journal of the Geological Society of Korea, 42(1), 79-94 (in Korean with English abstract).

Kim, Y. S. and Jin, K. M., 2007, Estimated earthquake magnitudes based of fault displacement data of Quaternary faults in SE Korea, Journal of Geology of Korea, 3, 57-78 (in Korean with English abstract).

Ko, M. S., Chang, C., Lee, J. B., and Shim, T. M., 2009, Application of coulomb stress model to the Odaesan Earthquake and its aftershock distribution, Journal of the Geological Society of Korea, 45(6), 741-750 (in Korean with English abstract).

Kyung, J. B., 2010, Paleoseismological study and evaluation of maximum earthquake magnitudes along the Yangsan and Ulsan fault zones in the southeastern part of Korea, Jigu-Mulli-wa-Mulli-Tamsa, 13(3), 187-197 (in Korean with English abstract).

Lee, C. G., 2014, Correlation analysis of rock properties and hazard distribution using 3d fem strike-slip fault model, MSc Thesis, Chungbuk National University, 15-19 (in Korean with English abstract).

Lin, J. and Stein, R. S., 2004, Stress triggering in thrust and subduction earthquakes, and stress interaction between the southern San Andreas and nearby thrust and strike-slip faults, Journal of Geophysical Research, 109 (B02303), 19p.

Mikumo, T. and Ando, M., 1976, A search into the faulting mechanism of the 1891 Great Nobi earthquake, Journal of Physics of the Earth, 24(1), 63-87.

Miyakoshi, J. I., Sato, T., and Fukuwa, N., 2003, Distribution of ground motion intensity evaluated using wooden house damage during the 1891 Nobi earthquake (M8) in central Japan, Institute of Social Safety Science, 5, 77-86 (in Japanese with English abstract).

Muramatsu, I., 1983, Distribution of the percentage of collapsed houses in the Nobi Plain for the Nobi earthquake of 1891, Research Report, Gifu University, 7, 867-882 (in Japanese with English abstract).

Nakano, M., Miyakoshi, J. I., and Yamaoka, K., 2007, A new model for the fault beneath the sedimentary basin in the 1891 Nobi earthquake, Earth Planets Space, 59, 13-19.

Seo, Y. S., Jang, H. S., and Chae, B. G., 2011a, Application of 3D FEM to fault-induced displacement models, Proceedings of the Korean Radioactive Waste Society 2011, 9(2), 445-446 (in Korean).

Seo, Y. S., You, Y. M., and Kim, K. Y., 2011b, 3D FEM analysis of fault-induced surface displacements, Proceedings of the Korean Radioactive Waste Society 2011, 9(2), 453-454 (in Korean).

Skempton, A. W. and McDonald, D. H., 1956, The allowable settlements of buildings, Proceedings ICE: Engineering Divisions, 5, 727-768.

Toda, S., Stein, R. S., Richards-Dinger, K., and Bozkurt, S., 2005, Forecasting the evolution of seismicity in southern California: Animations built on earthquake stress transfer, Journal of Geophysical Research, 110 (B05S16), 17p.

Wakita, K., Harayama, S., Kano, K., Mimura, K., and Sakamoto, T., 1992, 1:200,000 Geological Map, Gifu, Geological survey of Japan.

Yeon, K. H., Park, D. H., Chang, C. J., and Shim, T. M., 2010, Estimation of moment magnitudes of microearthquakes for probabilistic earthquake hazard evaluation, Proceedings of the 2010 Joint Symposium on Geosciences, 24p.

Young-Mook Choi
Department of Earth and Environmental Sciences, Chungbuk National University
52 Naesoodong-ro, Seowon-gu, Cheongju-si, Choongbuk Province, 362-763
Tel: 043-261-2765
E-mail: cym0831@nate.com

Woo-Seok Kim
Department of Earth and Environmental Sciences, Chungbuk National University
52 Naesoodong-ro, Seowon-gu, Cheongju-si, Choongbuk Province, 362-763
Tel: 043-261-2765
E-mail: peroxide@hanmail.net

Chul-Goo Lee
Department of Earth and Environmental Sciences, Chungbuk National University
52 Naesoodong-ro, Seowon-gu, Cheongju-si, Choongbuk Province, 362-763
Tel: 043-261-2765
E-mail: buuny@naver.com

Chang-Yong Kim
Geotechnical Engineering & Tunnelling Research Division, Korea Institute of Construction Technology (KICT), 283 Goyang-daero, Ilsanseo-gu, Goyang-si, Gyeonggi Province, 412-712
Tel: 031-910-0224
E-mail: cykim@kict.re.kr

Yong-Seok Seo
Department of Earth and Environmental Sciences, Chungbuk National University, 52 Naesoodong-ro, Seowon-gu, Cheongju-si, Choongbuk Province 362-763
Tel: 043-261-2765
E-mail: ysseo@cbu.ac.kr